INTERNATIONAL JOURNAL OF PRECISION ENGINEERING AND MANUFACTURING Vol. 18, No. 11, pp. 1495-1499 NOVEMBER 2017 / 1495

REGULAR PAPER

DOI: 10.1007/s12541-017-0177-2
ISSN 2234-7593 (Print) / 2005-4602 (Online)

Effect of the Chemical Composition on the Ablation Characteristics of Glass Substrates in Femtosecond Laser Machining

Hyeon-Min Lee[1], Jung Hyun Choi[2], and Seung-Jae Moon[1,#]

1 Department of Mechanical Engineering, Hanyang University, 222, Wangsimni-ro, Seongdong-gu, 04763, Seoul, South Korea
2 Department of Environmental Science and Engineering, Ewha Womans University, 52, Ewhayeodae-gil, Seodaemun-gu, 03760, Seoul, South Korea
Corresponding Author / E-mail: smoon@hanyang.ac.kr, TEL: +82-2-2220-0450, FAX: +82-2-2220-2299

KEYWORDS: Glass, Drilling, Femotosecond laser

In this work, we investigated the ablation characteristics of aluminosilicate, soda-lime, and borosilicate glass substrates in femtosecond laser processing. The laser wavelength was 1,552 nm with a pulse duration of 800 fs. The ablation threshold energy of each glass substrate was estimated using the D^2 method. To determine the ablation threshold energy of each glass substrate, the weight percentages of various chemical components in the glass substrates were quantitatively analyzed by laser ablation inductively coupled plasma mass spectrometry. The ablation threshold energy of the glass substrates was found to depend on the Al_2O_3 and MgO contents. When the weight percentages of both components were higher, the ablation threshold energy was lower. The effect of these components on the ablation threshold energy was theoretically investigated using self-trapped exciton analysis.

Manuscript received: September 6, 2016 / Revised: August 7, 2017 / Accepted: August 7, 2017

NOMENCLATURE

D = ablated crater diameter
Φ_{th} = threshold energy
Φ_0 = incident laser fluence
ω_0 = laser beam diameter

1. Introduction

Glass substrates are widely utilized for displays in electronic devices. However, the brittle nature of glass can cause random breaking, cracks, and chipping in conventional machining. These problems are detrimental to the productivity and quality of products. Femtosecond laser machining can overcome the disadvantages of conventional mechanical machining because a very small heat-affected zone (HAZ) is created by an extremely high energy density of ultra-short laser pulses. Laser machining using a femtosecond laser is known as an efficient tool for the precise micromachining of strengthened glass substrates such as aluminosilicate, soda-lime, and borosilicate glass substrates. However, laser machining quality needs to be improved for industrial applications since the industry demands high quality and faster machining speed when employing femtosecond laser machining. There have been numerous recent studies that have intensively investigated laser machining. In-depth studies to reveal the interaction mechanism of incident laser energy with dielectric materials (i.e., silicon dioxide, glass, and sapphire) have been carried out by many research groups.[1-3] These have focused on the morphology of ablated craters with various incident laser energies to experimentally obtain the ablation threshold energy of each dielectric material.[4] Numerical simulation of the ablation process was performed to examine the relationship between the incident laser energy and crater morphology.[1-3,5,6] Recently, Butkus and Gaizauskas presented results on the rapid microfabrication of transparent materials (soda-lime glass and Corning® Gorilla® glass) using femtosecond laser pulses and examined the differences of the machining characteristics of femtosecond laser machining.[6] They found that a different laser scanning speed was required to achieve a drilling depth of 3 mm for each type of glass substrate with the same laser fluence of 6.6 J/cm^2. Moreover, the band gap energy of soda-lime glass (2.6 eV) is lower than that of Gorilla® glass (3.5 eV).[7,8] To achieve a drilling depth of 3 mm, the

required scanning speed of soda-lime glass (100 mm/s) was lower than that of Gorilla® glass (400 mm/s). In drilling a hole in the soda-lime glass substrate, the low scanning speed is required to provide a higer laser energy than the energy needed to drill the same depth hole in the Gorilla glass substrate at the same laser intensity, even though soda-lime glass has a lower band gap energy. In the glass industry, it is known that the chemical components of each type of multi-component glass are different since the inclusion of chemical components in glass is tailored for different applications. Aluminosilicate, soda-lime, and borosilicate substrates are widely adopted for display glass in various electric devices, including mobile smartphones, tablets, and laptops. Aluminosilicate glass (ASG, Corning® Gorilla® glass) has a higher content of Al_2O_3 than other glass substrates because the inclusion of Al_2O_3 can increase its strength, scratch resistance, and durability.[9] Soda-lime glass (SLG) manufactured by Asahi® is known to have higher concentrations of Na_2O and CaO. Soda-lime glass substrates are used for liquid crystal display (LCD) panels, windowpanes, and glass containers because of its relatively affordable price, chemical stability, and recyclability.[10] Borosilicate glass (BSG, Corning® Eagle XG® glass, 3.5 eV) is manufactured without the use of heavy metal ions. This glass has high surface quality and excellent thermal properties for more advanced LCD displays.[11]

In this work, we experimentally investigated the laser-machining characteristics of aluminosilicate, soda-lime, and borosilicate glass substrates to determine the threshold laser energy of each glass substrate. To investigate the different characteristics of the threshold laser energy, quantitative analysis of the chemical composition was carried out. The ablation threshold energy is critical for the purpose of achieving precise machining by determining the initial energy input. The ablated crater morphology of each substrate was investigated to determine the threshold energy of each substrate by varying the laser fluence. The chemical components of the glass substrates were quantitatively obtained by laser ablation inductively coupled plasma mass spectrometry (LA-ICP MS). The effects of various chemical components (except for SiO_2) on the ablation characteristics of each glass substrate can be explained in terms of the behavior of the free electrons of alkali metals in the conduction bands during femtosecond laser machining.

2. Experiments

For the experimental sample preparation, the glass substrates were sufficiently washed using methanol (CH_3OH) and completely dried with lens tissues and a clean air shower to remove any remaining pollutants on the surfaces of the substrates. One-shot ablation experiments to estimate the ablation threshold energy were carried out with 400 μm thick glass substrates by irradiating a laser pulse at a wavelength of 1,552 nm for 800 fs. These glass substrates were positioned normal to the incoming laser pulse under ambient conditions, as shown in Fig. 1. The laser beam diameter, which was tightly focused by an objective lens, was determined to be 3 μm using the D^2 method.[12] In this method, the threshold energy for the laser ablation of each glass substrate can be accurately obtained from the intercepts of the slope on the horizontal axis of the laser fluence. The laser energy absorbed into the substrates was measured by an optical power meter before the ablation experiment.

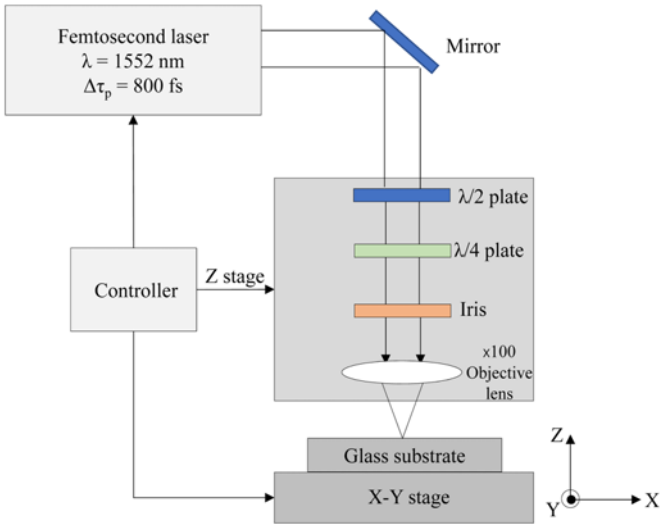

Fig. 1 Schematic diagram of a glass substrate micromachining

The ablated crater morphology on the substrates was observed using a three-dimensional laser scanning microscope (Keyence® VK-9710K model). The resolution specification of this system was precise enough to observe changes of the crater shape on the scale of 1 nm. The contents of the chemical components of the glass substrates were analyzed using laser ablation inductively coupled plasma mass spectrometry (LA-ICP MS) with the irradiation of an ultra-violet Yttrium laser at a pulse duration of 500 fs and a wavelength of 342 nm. The beam size was 75 μm and the spectrometer ranged from 200 to 890 nm.

3. Results and Discussion

The ablated crater morphologies of each substrate obtained from the top view are shown in Fig. 2. The crater morphologies of each substrate were created by single shot ablation at laser fluences of 9.8, 12.2, 14.6, and 16.2 J/cm^2. The crater diameters increased from 2.3 μm to 5.5 μm in borosilicate glass, 4.6 μm to 6.5 μm in aluminosilicate glass, and 3.6 μm to 7.0 μm in soda-lime glass, as the laser fluence was increased from 9.8 to 16.2 J/cm^2. The heat affected zone can be clearly observed at the outside of the ablated crater even though a femtosecond laser was adopted. Since the beam profile of the irradiated laser beam has a Gaussian profile extending from negative infinity to positive infinity, the radius corresponding to the ablation threshold laser energy increased with increasing laser fluence. The crater diameters of each substrate increased with increasing laser fluence since the laser beam radius is defined as the radius at 1/e^2 from the maximum laser energy value.

$$2\omega_0^2 = \frac{D^2}{\ln(\phi_0) - \ln(\phi_{th})} \quad (1)$$

Fig. 3 presents the squared ablated crater diameters of each substrate obtained with various laser fluences. To investigate the differences of the crater morphology of each glass substrate for the various laser fluences, the laser threshold energy was estimated by the *D*-squared method (D^2).[12,13] The threshold fluence (Φ_{th}) in each glass substrate can be estimated from the relationship between the incident laser fluence (Φ_0), laser beam radius (ω_0), and crater diameter (D) in Eq. (1). The

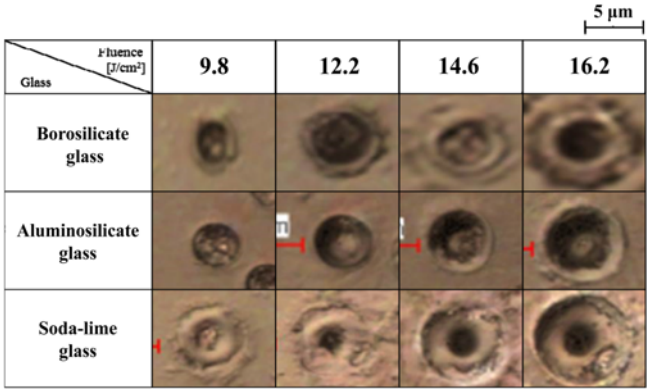

Fig. 2 Ablated crater morphology and diameter of each glass created with laser fluences of 9.8, 12.2, 14.6, and 16.2 J/cm^2

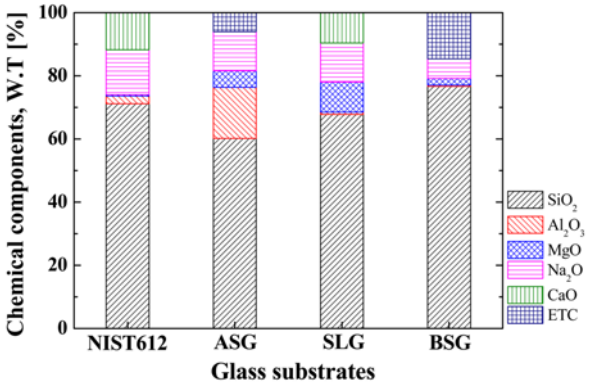

Fig. 4 Chemical components contained in each industrial glass as determined by LA-ICP MS measurement

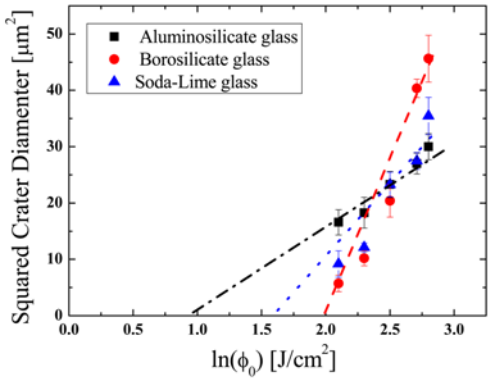

Fig. 3 Ablation threshold energy obtained by the D^2 method for each glass substrate

slope of the fitted line between the logarithmic incident laser fluence and the squared crater diameter is the twice of the squared laser beam radius from Eq. (1). Fig. 3 shows the slight deviation of the experimentally obtained squared crater diameters from the linear curves. This deviation is known to be caused by the thermal effect.[12] The D^2 method is derived under the assumption that no thermal effect is involved in the ablation process. This deviation may be caused by the thermal effect induced from the impurities. This will be discussed later. The laser fluence of a single laser pulse was varied from 9.8 to 16.2 J/cm^2 and the average crater diameters obtained from ten experimental results at each laser fluence are presented with a corresponding error bar. The aluminosilicate glass substrate had the lowest average threshold laser fluence of 2.53 J/cm^2. The variation of the threshold laser fluence in the aluminosilicate glass was from 2.1 J/cm^2 to 2.9 J/cm^2. The average threshold laser fluence of soda-lime glass was 5.34 J/cm^2 (4.9-5.7 J/cm^2). The highest threshold laser fluence of 7.23 J/cm^2 was obtained for the borosilicate glass substrate (6.8-7.7 J/cm^2).

Fig. 4 shows the weight percentages (wt.%) of the chemical components contained in each substrate. To investigate the differences of the ablation characteristics and the threshold energy, the weight percent of the chemical components in each type of glass substrate was determined by LA-ICP MS. In the LA-ICP MS measurement, the various chemical components can be quantitatively obtained by comparing the peak intensities at the characteristic wavelength of each element. To prove the accuracy of the quantitative chemical component measurement, the intensity peak values of NIST 612 standard glass obtained from the LA-ICP MS measurement were used as a reference. The spectra of Si, Al, Na, Mg, and Ca were selected because they are known to be abundant in glass and the reference glass sample (NIST 612) has known weight percentages of each selected element.[14,15] Their oxidized compounds of SiO_2, Al_2O_3, MgO, Na_2O, and CaO are known to be abundant in glass substrates. Aluminosilicate glass has a higher Al_2O_3 content of 17 wt.% than other types of glass (<5 wt.%).[9-11] High weight percentages of Na_2O and CaO are present in soda-lime glass (16 wt.% Na_2O and 9.5 wt.% CaO). Borosilicate glass had low weight percentages of Na_2O and CaO compared to the other types of glass. In femtosecond laser ablation, ablation mechanisms include nonlinear optical absorption (which is caused by multiphoton ionization), avalanche breakdown, and Coulomb explosion. These strongly nonlinear absorption processes can enhance the localization of the excitation energy on the surface of materials. Therefore, wide bandgap materials can be ablated with femtosecond lasers, although these materials have low absorptivity at wavelengths greater than 250 nm. The ablation process within wide bandgap materials occurs when the density of free electrons in the conduction band exceeds a critical number density ($O(10^{21}$ cm^{-3})).[16] For Al_2O_3 and MgO components, the relaxation time scales of the free carrier electrons in the conduction band are known to be longer than those of other components.[17] The lifetimes of free carrier electrons in the conduction bands provided by various wide bandgap oxides such as SiO_2, Al_2O_3, and MgO have been evaluated in previous research.[18,19] The free electrons of Al_2O_3 and MgO remain for several tens of picoseconds in the conduction band, whereas those of SiO_2 remain for just 100 femtoseconds. The relaxation time scale of the free electrons of Al_2O_3 and MgO is two orders greater than that of the free electrons of SiO_2.

Self-trapped exciton (STE) formation is known to occur during the interaction of femtosecond laser pulses with wide bandgap dielectrics.[20,21] STE formation leads to the localization of thermal energy caused by self-trapped carriers. The transferred energy produces energetic atoms. These atoms can produce defect formations in a lattice, i.e., interstitials or vacancies. The STE formation suppresses additional electron excitation and triggers the relaxation process. The relaxation time of the excited electrons is known to be dependent on the material. In the STE formation

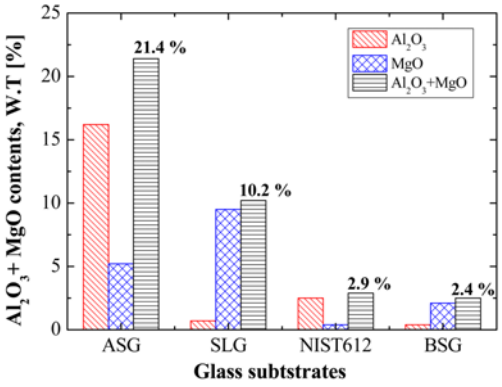

Fig. 5 The summation of Al_2O_3 and MgO (wt.%) in ASG, SLG, NIST 612, and BSG glass substrates

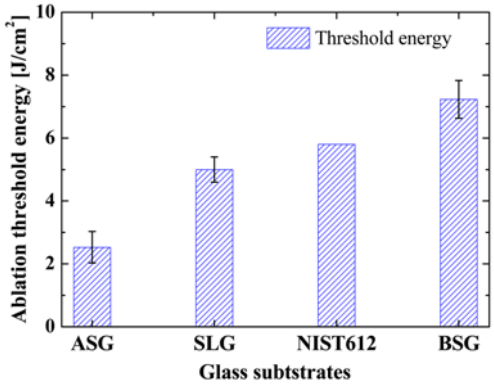

Fig. 6 The ablation threshold fluence (J/cm^2) in ASG, SLG, NIST 612,[21,22] and BSG glass substrates

mechanism, an electron-hole pair is generally created by incident radiation of the laser beam. The molecular ion formation results from the self-trapping of a hole in less than 1 ps. An electron is then captured by a hole to form the STE. The STEs will not be formed if the relaxation time of excited electrons exceeds that of the STE formation. According to previous research involving a diamond, MgO, and Al_2O_3, the relaxation time scale is around several tens of picoseconds without trapping.[17] On the other hand, the relaxation time scale is approximately 150 fs in NaCl, KBr, and SiO_2. When the STE relaxation time is greater than the lattice relaxation time scale of 10 ps, the released energy from the excited free electrons is converted to lattice heat energy. This will expedite the phonon creation for heat transfer around the irradiated spot. The containment of Al_2O_3 and MgO may be conducive to the formation of the heat affected zone around the ablated crater. The Al_2O_3 and MgO components have thermal characteristics to convert the released laser energy to lattice heat energy.

Therefore, the deviation of the squared measured crater diameter from the linear fitted line estimated by the D^2-method was caused by this additional heat transfer mechanism. The different deformation potential ratio and elastic constant (Young's modulus) of the materials affect the relaxation time of a material.[19] Self-trapping phenomena can be observed in materials with high deformation potential ratios and small elastic constants. The self-trapping probability can be increased with higher deformation potential ratios and smaller elastic constants. The elastic constant of SiO_2 (87 GPa) is much smaller than those of Al_2O_3 (497 GPa) and MgO (297 GPa). The probabilities of STE formation in Al_2O_3 and MgO are lower than that of SiO_2, and the relaxation times of free electrons in the conduction bands of Al_2O_3 and MgO are much longer than those in the conduction band of SiO_2.[19]

Fig. 5 shows the summation of the Al_2O_3 and MgO weight percentages contained in ASG, SLG, NIST612, and BSG substrates and Fig. 6 presents the corresponding average ablation threshold laser fluences. The sum of the Al_2O_3 and MgO contents are 21.4 wt.% in ASG, 10.2 wt.% in SLG, 2.9 wt.% in NIST612, and 2.4 wt.% in BSG in Fig. 5. The order of the ablation threshold fluences was inversely proportional to the order of the summation of the Al_2O_3 and MgO contents in each glass substrate in Fig. 6. The laser ablation threshold fluence and contained component information of NIST612 were obtained from the literature.[22,23] The weight percentages of Al_2O_3 and MgO measured by LA-ICP MS were 2 wt.% and 0.9 wt.%, respectively. The ablation threshold energy is about 5.5 J/cm^2 with the irradiation of a femtosecond pulsed laser at the wavelength of 1,552 nm.[22,23] The employed laser wavelength of 1,552 nm is the same as the wavelength adopted in this work. As the weight percentages of the Al_2O_3 and MgO components in each glass substrate decreased, the ablation threshold energy levels increased. The BSG substrate with a lower weight percent (2.4 wt.%) of the Al_2O_3 and MgO components demonstrated a higher average ablation threshold fluence of 7.23 J/cm^2 because of the STE formation. In NIST612, the ablation laser fluence is 5.5 J/cm^2 and the summation of Al_2O_3 and MgO content is 2.9 wt.%. In SLG, the average laser fluence is 5.34 J/cm^2 and the summation of Al_2O_3 and MgO content is 10.2 wt.%. The ASG substrate shows the lowest laser fluence of 2.53 J/cm^2 with a summation of Al_2O_3 and MgO content of 21.4 wt.%. As the Al_2O_3 and MgO components have a longer relaxation time scale of several tens of picoseconds, the heat irradiated during relaxation will be transferred to the glass substrate around the irradiated spot. Therefore, the ASG with higher Al_2O_3 and MgO contents could reach the critical energy density for ablation at a lower threshold energy. Since NIST 612 and BSG have lower Al_2O_3 and MgO contents compared to ASG and SLG, the ablation threshold fluences of NIST 612 and BSG are higher than those of ASG and SLG. In previous research, the scanning speed of soda-lime glass was shown to be lower than that of ASG to obtain grooves with the same depth.[6] The low scanning speed means that SLG needs a higher laser energy to reach the critical electron density for ablation.

4. Conclusions

In this work, the difference of the ablation threshold laser fluences of glass substrates was investigated by employing quantitative analysis of the chemical components of ASG, SLG, and BSG substrates. As the weight percent of the Al_2O_3 and MgO components in the glass substrates increased, less ablation threshold energy is required. ASG with 21.4 wt.% of Al_2O_3 and MgO had the lowest average ablation threshold fluence of 2.53 J/cm^2. The threshold energy of SLG with 10.2 wt.% of Al_2O_3 and MgO was 5.34 J/cm^2 and that of BSG with 2.4 wt.% of Al_2O_3 and MgO was 7.23 J/cm^2. The threshold energy was inversely dependent on

the sum of the weight percentages of Al_2O_3 and MgO contained in each substrate.

ACKNOWLEDGMENT

This work was supported by the National Research Foundation of Korea (NRF) grant funded by the Korea government (No. NRF-2016 R1D1A1B03935556).

REFERENCES

1. Lenzner, M., Krüger, J., Sartania, S., Cheng, Z., Spielmann, C., et al., "Femtosecond Optical Breakdown in Dielectrics," Physical Review Letters, Vol. 80, No. 18, pp. 4076-4079, 1998.
2. Jia, T., Li, R., Liu, Z., Chen, H., and Xu, Z., "Threshold of Ultra-Short Pulse Laser-Induced Damage in Dielectric Materials," Applied Surface Science, Vol. 189, No. 1, pp. 78-83, 2002.
3. Perry, M. D., Stuart, B. C., Banks, P. S., Feit, M. D., Yanovsky, V., and Rubenchik, A. M., "Ultrashort-Pulse Laser Machining of Dielectric Materials," Journal of Applied Physics, Vol. 85, No. 9, pp. 6803-6810, 1999.
4. Krüger, J., Kautek, W., Lenzner, M., Sartania, S., Spielmann, C., and Krausz, F., "Laser Micromachining of Barium Aluminium Borosilicate Glass with Pulse Durations between 20 fs and 3 ps," Applied Surface Science, Vols. 127-129, pp. 892-898, 1998.
5. Schaffer, C. B., Brodeur, A., and Mazur, E., "Laser-Induced Breakdown and Damage in Bulk Transparent Materials Induced by Tightly Focused Femtosecond Laser Pulses," Measurement Science and Technology, Vol. 12, No. 11, pp. 1784-1749, 2001.
6. Butkus, S., Gaižauskas, E., Paipulas, D., Viburys, Ž., Kaškelyė, D., et al., "Rapid Microfabrication of Transparent Materials Using Filamented Femtosecond Laser Pulses," Applied Physics A, Vol. 114, No. 1, pp. 81-90, 2014.
7. Russ, S., Siebert, C., Eppelt, U., Hartmann, C., Faißt, B., and Schulz, W., "Picosecond Laser Ablation of Transparent Materials," Proc. of SPIE, Paper No. 86080E, 2013.
8. Ruengsri, S., Kaewkhao, J., and Limsuwan, P., "Optical Characterization of Soda Lime Borosilicate Glass Doped with TiO_2," Procedia Engineering, Vol. 32, pp. 772-779, 2012.
9. Corning, "Gorilla Glass Product Information," http://www.corning.com/microsites/csm/gorillaglass/PI_Sheets/CGG_PI_Sheet_Gorilla%20Glass%203.pdf (Accessed 30 OCT 2017)
10. Asano, Y., "AGC Glass Technology Solutions for High Performance and Functional Display Requirements," http://www.sid.org/Portals/5/pdf/AGC_Asahi_Glass_DW2013.pdf (Accessed 17 OCT 2017)
11. Corning, "Industry-Leading LCD Glass Substrates for evolving Displays," http://www.corning.com/worldwide/en/products/display-glass/products/eagle-xg-slim.html (Accessed 17 OCT 2017)
12. Liu, J., "Simple Technique for Measurements of Pulsed Gaussian-Beam Spot Sizes," Optics Letters, Vol. 7, No. 5, pp. 196-198, 1982.
13. Von der Linde, D., and Schüler, H., "Breakdown Threshold and Plasma Formation in Femtosecond Laser-Solid Interaction," Journal of the Optical Society of America B, Vol. 13, No. 1, pp. 216-222, 1996.
14. Wang, C. and Zimmer, J., "Aluminosilicate Glass for Touch Screen," US Patent, 20130202715 A1, 2010.
15. National Institute of Standards and Technology, "Material Deails: SRM 612-Trace Elements in Glass," https://www-s.nist.gov/srmors/view_detail.cfm?srm=612 (Accessed 17 OCT 2017)
16. Bauerle, D. W., "Laser Processing and Chemistry," 2011.
17. Mao, S., Quér, F., Guizard, S., Mao, X., Russo, R., et al., "Dynamics of femtosecond Laser Interactions with Dielectrics," Applied Physics A: Materials Science & Processing, Vol. 79, No. 7, pp. 1695-1709, 2004.
18. Guizard, S., Martin, P., Daguzan, P., Petite, G., Audebert, P., et al., "Contrasted Behaviour of an Electron Gas in MgO, Al_2O_3 and SiO_2," Europhysics Letters, Vol. 29, No. 5, pp. 401-406, 1995.
19. Martin, P., Guizard, S., Daguzan, P., Petite, G., D'oliveira, P., et al., "Subpicosecond Study of Carrier Trapping Dynamics in Wide-Band-Gap Crystals," Physical Review B, Vol. 55, No. 9, pp. 5799-5810, 1997.
20. Quér, F., Guizard, S., and Martin, P., "Time-Resolved Study of Laser-Induced Breakdown in Dielectrics," Europhysics Letters, Vol. 56, No. 1, pp. 138-144, 2001.
21. Grigoropoulos, C. P., "Transport in Laser Microfabrication: Fundamentals and Applications," Cambridge University Press, 2009.
22. Jia, T. Q., Chen, H. X., Huang, M., Zhao, F. L., Li, X. X., et al., "Ultraviolet-Infrared Femtosecond Laser-Induced Damage in Fused Silica and CaF_2 Crystals," Physical Review B, Vol. 73, No. 5, Paper No. 054105, 2006.
23. LaHaye, N. L., Harilal, S. S., Diwakar, P. K., Hassanein, A., and Kulkarni, P., "The Effect of Ultrafast Laser Wavelength on Ablation Properties and Implications on Sample Introduction in Inductively Coupled Plasma Mass Spectrometry," Journal of Applied Physics, Vol. 114, No. 2, Paper No. 023103, 2013.